

**This is the Accepted Author Manuscript of the following publication:**

Boutin H, Murray K, Pradillo J, Maroy R, Smigova A, Gerhard A, Jones PA, Trigg W. (18)F-GE-180: a novel TSPO radiotracer compared to (11)C-R-PK11195 in a preclinical model of stroke. *Eur J Nucl Med Mol Imaging*. 2015 Mar;42(3):503-11. doi: 10.1007/s00259-014-2939-8. Epub 2014 Oct 29.

**The final publication is available at:**

<http://link.springer.com/article/10.1007%2Fs00259-014-2939-8>

**<sup>18</sup>F-GE-180: a novel TSPO radiotracer compared to <sup>11</sup>C-R-PK11195  
in a preclinical model of stroke.**

Hervé Boutin<sup>1,2</sup>, Katie Murray<sup>3</sup>, Jesus Pradillo<sup>3,4\*</sup>, Renaud Maroy<sup>5</sup>, Alison Smigova<sup>2</sup>,  
Alexander Gerhard<sup>1,2</sup>, Paul A. Jones<sup>6</sup>, William Trigg<sup>6</sup>.

<sup>1</sup> Faculty of Medical and Human Sciences, University of Manchester, Manchester, UK.

<sup>2</sup> Wolfson Molecular Imaging Centre, University of Manchester, Manchester, UK.

<sup>3</sup> Faculty of Life Sciences, University of Manchester, Manchester, UK.

<sup>4</sup> Present address: Universidad Complutense/Politecnica de Madrid, Madrid, Spain

<sup>5</sup> SHFJ - CEA Orsay, France.

<sup>6</sup> GE Healthcare Ltd., Amersham, UK.

**Corresponding author:** Dr Hervé Boutin, Senior Research Scientist, University of Manchester, Wolfson Molecular Imaging Centre, 27 Palatine Road, Manchester, M20 3LJ – UK; Tel.: +44 (0) 161 275 0078; FAX: +44 (0)161 275 0003; email: herve.boutin@manchester.ac.uk

**Word count:** 5233

**Running title:** <sup>18</sup>F-GE-180: A novel TSPO radiotracer.

## 1 ABSTRACT

2 **Purpose:** Neuroinflammation plays a critical role in various neuropathological  
3 conditions, hence the regain of interest for the translocator protein (TSPO) as  
4 biomarker of microglial activation and macrophage infiltration in the brain. This is  
5 illustrated by the large amount of research conducted to replace the prototypical  
6 positron emission tomography (PET) radiotracer  $^{11}\text{C}$ -R-PK11195 by a higher  
7 performance TSPO ligand. Here we are reporting the in vivo preclinical investigation  
8 of the novel TSPO tracer  $^{18}\text{F}$ -GE-180 in a model of stroke in rats.

9 **Methods:** Sixty minutes middle cerebral artery occlusion (MCAO) was  
10 induced in Wistar rats. Twenty-four hours post-MCAO, brain damages were  
11 assessed by  $T_2$  MRI. Rats were scanned with  $^{11}\text{C}$ -R-PK11195 and  $^{18}\text{F}$ -GE-180 five  
12 or six days post-MCAO. Specificity of the binding was confirmed by injection of  
13 unlabelled R-PK11195 or GE-180 20min post-injection of  $^{18}\text{F}$ -GE-180. In vivo data  
14 were confirmed by ex vivo immunohistochemistry (IHC) for microglial (CD11b) and  
15 astrocytic biomarkers (GFAP).

16 **Results:**  $^{18}\text{F}$ -GE-180 uptake was 24% higher in the core of the ischemic  
17 lesion and 18% lower in the contralateral healthy tissue than  $^{11}\text{C}$ -R-PK11195 uptake  
18 ( $1.5 \pm 0.2$  fold higher signal to noise ratio). We confirmed this finding using the  
19 simplified reference tissue model ( $\text{BP}_{\text{ND}} = 3.5 \pm 0.4$  vs.  $2.4 \pm 0.5$  for  $^{18}\text{F}$ -GE-180 than for  
20  $^{11}\text{C}$ -R-PK11195 respectively, with  $R_1 = \frac{k_1}{k_1'} = 1$ ). Injection of unlabelled R-PK11195 or  
21 GE-180 20min post-injection of  $^{18}\text{F}$ -GE-180 displaced significantly  $^{18}\text{F}$ -GE-180  
22 binding ( $69\% \pm 5\%$  and  $63\% \pm 4\%$ , respectively). Specificity of the binding was also  
23 confirmed by in vitro autoradiography, whereas location and presence of activated  
24 microglia and infiltrated macrophages was confirmed by IHC.

1           **Conclusions:** The in vivo binding characteristic of  $^{18}\text{F}$ -GE-180 demonstrate a  
2 better signal to noise ratio than  $^{11}\text{C}$ -R-PK11195 due to both a better signal in the  
3 lesion and also lower non-specific binding in healthy tissue. These results provide  
4 evidence that  $^{18}\text{F}$ -GE-180 is a strong candidate to replace  $^{11}\text{C}$ -R-PK11195.

5           **Keywords:** positron emission tomography; translocator protein; R-PK11195; brain  
6 ischemia; GE-180.

# 1 INTRODUCTION

2 Over the past decades, increasing evidence has supported the role of  
3 neuroinflammation as an essential contributor in CNS diseases, whether it is acute  
4 brain injury such as stroke [2;3], chronic neurodegenerative diseases such  
5 Alzheimer's disease [4-8], Parkinson's disease [9-12] or primary inflammatory  
6 disorders like multiple sclerosis [13-15]. This has led to an increasing interest in  
7 visualising neuroinflammation in a non-invasive manner that would allow better  
8 understanding of neuroinflammation, its time course and role in brain diseases. So  
9 far, the most established and best characterised biomarker for in vivo imaging of  
10 neuroinflammation is the translocator protein 18kDa (TSPO), formerly known as  
11 peripheral benzodiazepine receptor (PBR) [16]. Strictly speaking, TSPO over-  
12 expression reflects microglial cell activation and proliferation [17] rather than  
13 neuroinflammation in its broader sense. TSPO characteristics as surrogate marker of  
14 neuroinflammation led to the development of  $^{11}\text{C}$ -R-PK11195 as a TSPO PET ligand  
15 in the early 80's [16;18].  $^{11}\text{C}$ -R-PK11195 has de facto the short half-life of C-11, a  
16 relatively poor signal to noise ratio due to high non-specific binding (for review see  
17 Chauveau *et al.* [16]) and a rather problematic radiochemistry, although this later  
18 point is poorly documented despite being well known by the radiochemistry  
19 community. To compensate for the poor binding properties of  $^{11}\text{C}$ -R-PK11195,  
20 advanced modelling techniques have been implemented in order to extract as much  
21 as possible information from the PET images when no anatomical reference tissue  
22 can be defined [19-21]. For these reasons and its long-lasting presence in the field of  
23 clinical TSPO PET imaging,  $^{11}\text{C}$ -R-PK11195 is still the most used TSPO radiotracer  
24 used in clinical studies [16]. However, over the last decade,  $^{11}\text{C}$ -R-PK11195 issues  
25 and the increased interest in neuroinflammation have triggered a renewed effort to

1 develop improved TSPO PET tracers and numerous compounds have been  
2 developed in this period [16;22;23]. Most of these tracers, such as <sup>18</sup>F-FEDAA1106,  
3 <sup>11</sup>C-PBR28, <sup>11</sup>C-DPA-713 or <sup>18</sup>F-DPA-714, have a better signal to noise ratio than  
4 <sup>11</sup>C-R-PK11195 in PET images of various animal models [16;24]. However, some of  
5 these studies clearly indicate variable results between different models and the need  
6 to perform direct comparison of the two tracers (i.e. same animal or subject scanned  
7 twice) [16;24;25]. More recently, these new tracers are being implemented in various  
8 clinical studies, sometimes yielding different results depending on the tracer used  
9 [15;26] or the disease studied [26;27].

10 Taken altogether, the preclinical and first clinical studies mentioned earlier  
11 highlight the need for thorough evaluation of these new tracers to expect some of  
12 them to be implemented at clinical level on a wider scale. Initial preclinical evaluation  
13 should provide information about the potential of a new TSPO PET tracer, but do not  
14 warrant success in the clinic. Ideally, a clinical evaluation of the tracer should follow,  
15 comparing any new tracer with <sup>11</sup>C-R-PK11195 in a disease for which the microglial  
16 activation is sufficiently described to prevent any bias.

17 We are here reporting the in vivo evaluation of a new tetrahydrocarbazole  
18 TSPO tracer, <sup>18</sup>F-GE-180 (S-N,N-diethyl-9-2-<sup>18</sup>F-fluoroethyl]-5-methoxy 2,3,4,9-  
19 tetrahydro-1H-carbazole-4-carboxamide [28], and its direct comparison (i.e. in the  
20 same animals) with <sup>11</sup>C-R-PK11195 in a rat model of stroke. To put our study into  
21 context, we have also compared our data with those recently published by Dickens  
22 *et al.* [1], *which compared the 2 tracers in different group of animals, in a different*  
23 *model of neuroinflammation (i.e. stroke vs LPS) and to provide novel information*  
24 *about the metabolism of <sup>18</sup>F-GE-180.*

# 1 MATERIALS AND METHODS

## 2 *Induction of Focal Cerebral Ischemia in Rats*

3 Studies were conducted on male Wistar rats (n=10) (Charles River, Margate,  
4 Kent, UK). Animals weighted 357±44g. The animals were kept under a 12h light–  
5 dark cycle with free access to food and water. All procedures were carried out in  
6 accordance with the Animals (Scientific Procedures) Act 1986, the specific project  
7 licence was approved by the UK Home Office. Focal cerebral ischemia was induced  
8 by 60min transient occlusion of the right middle cerebral artery (MCAO) by the  
9 insertion of a monofilament (DOCCOL Corp.) as previously described [24] (for full  
10 details see supplementary material).

## 11 *Magnetic Resonance Imaging*

12 The primary outcome was infarct volume measured by MRI 24h after transient  
13 MCAO. Animals were scanned using a Magnex 7-Tesla, horizontal-bore magnet  
14 (Agilent Technologies, Oxford Industrial Park, Yarnton, Oxford, UK) connected to a  
15 Bruker Biospec Avance III console (Bruker Biospin Ltd, Banner Lane, Coventry, UK )  
16 with a transmit/receive 2.5cm surface coil. Rectal temperature and respiration rate  
17 were monitored. Reperfusion of the right MCA was assessed using a FLASH-TOF-  
18 2D sequence. A T<sub>2</sub>-weighted fast spin echo sequence based on RARE was used to  
19 measure brain damage [29;30] (details of the sequences can be found in  
20 supplementary material). Lesion volume was determined with Anatomist software  
21 (<http://brainvisa.info/>), ROIs corresponding to the infarcted tissue were delineated on  
22 the T2 MRI based on the enhanced contrast of oedematous tissue when compared  
23 with healthy tissue 24h post-MCAO.

## 1 ***Positron Emission Tomography Scans and Data Acquisition***

2 Five to six days after MCAO, rats were anaesthetized by isoflurane inhalation  
3 (induction: 5% and thereafter 2-2.5%) in oxygen. As control, naive rats (no MCAO)  
4 were scanned with  $^{18}\text{F}$ -GE-180 (n=5). All compounds were injected intravenously in  
5 the tail vein as a bolus. All injected doses, amount of tracer injected and specific  
6 activity are provided in supplementary table 1.

## 7 **Dual Scans $^{11}\text{C}$ -R-PK11195 - $^{18}\text{F}$ -GE-180**

8 Six animals were scanned sequentially with  $^{11}\text{C}$ -R-PK11195 and  $^{18}\text{F}$ -GE-180  
9 within 24h (4 rats were scanned with  $^{11}\text{C}$ -R-PK11195 first and then with  $^{18}\text{F}$ -GE-180  
10 (3h to 6h later) and 2 rats were scanned with  $^{18}\text{F}$ -GE-180 first and with  $^{11}\text{C}$ -R-  
11 PK11195 the following day).  $^{11}\text{C}$ -R-PK11195 and  $^{18}\text{F}$ -GE-180 were synthesized as  
12 described elsewhere [28;31;32].

## 13 **Displacement Study**

14 To assess the specificity of  $^{18}\text{F}$ -GE-180 in vivo, a displacement study was  
15 performed by injecting an excess (1mg/kg) of either unlabelled R-PK11195 or GE-  
16 180 during the PET acquisition twenty minutes following the injection of  $^{18}\text{F}$ -GE-180.  
17 Three rats were scanned twice with  $^{18}\text{F}$ -GE-180 within 24h, once with administration  
18 of unlabelled R-PK11195 and once following administration of GE-180 as unlabelled  
19 ligand 20min post-injection of  $^{18}\text{F}$ -GE-180.

## 20 **Data Acquisition**

21 The scans were performed on a Siemens Inveon® PET-CT scanner. A CT  
22 scan was performed prior the PET acquisition to obtain the attenuation correction  
23 factors. The list mode acquisition data files were histogrammed into 3D sinograms



1 and reconstructed using OSEM3D (details of the PET protocols can be found in  
2 supplementary material).

3         Respiration and temperature were monitored throughout using a pressure  
4 sensitive pad and rectal probe (BioVet, m2m imaging corp, USA). Body temperature  
5 was maintained ( $37\pm 0.7^{\circ}\text{C}$ ) by use of a heating and fan module controlled by the  
6 rectal probe via the interface controlled by the BioVet system.

7         At the end of the last PET scan, rats were quickly decapitated and the brains  
8 were quickly removed and immediately frozen in isopentane in dry ice. The brains  
9 were stored at  $-80^{\circ}\text{C}$  until cut with cryomicrotome in adjacent  $20\mu\text{m}$  thick coronal  
10 sections. Brain sections were then stored at  $-80^{\circ}\text{C}$  until used for autoradiography or  
11 immunohistochemistry.

## 12         ***Image Analysis***

13         PET images were analysed using two sets of ROIs. The first set of ROI came  
14 from the automatic segmentation of the PET images using the Local Means Analysis  
15 (LMA) method [33] with Partial Volume Effect (PVE) correction using the Geometric  
16 Transfer Matrix (GTM) method and the ROlopt methods [24;33-35]. Automatic  
17 segmentation of the volume had the advantage of delineating user-independent  
18 ROIs. For both tracers the following five ROIs were automatically segmented and  
19 labelled as: (1) core (ROI covering the core of the infarct in the MCAO territory  
20 and/or with the highest uptake), (2) edge-1 (ROI around the core ROI and/or with the  
21 second highest uptake), (3) edge-2 (ROI around the core ROI and/or with the 3<sup>rd</sup>  
22 highest uptake), (4) edge-3 (ROI around the core ROI and/or with the 4<sup>th</sup> highest  
23 uptake), (5) contralateral ROI (ROI with the lowest uptake) and (6) skull edges (6<sup>th</sup>  
24 ROI located on the edge of the skull, this ROI was not included in the data analysis).

1 In control animal, two ROIs within the whole brain were segmented corresponding to  
2 a higher uptake ROI near the cerebroventricular zones and a lower uptake ROI  
3 corresponding to the rest of the brain (data not shown). The second set of ROIs was  
4 obtained from the anatomical ROIs used for the quantification of the infarct volume  
5 on the T2 images (as described in the Magnetic resonance imaging section). To co-  
6 register the T2 MR and PET-CT images, a brain mask was delineated on each  
7 individual T2 MRI and CT images, the resulting brain masks were then co-registered  
8 using rigid registration with mutual information. All methods were applied using the  
9 BrainVisa/Anatomist framework (<http://brainvisa.info/>).

10 The cerebellum and olfactory bulbs were delineated based on the co-  
11 registered MRI.  $^{11}\text{C}$ -R-PK11195 and  $^{18}\text{F}$ -GE-180 uptake was quantified using both  
12 the segmented and MRI-based ROIs.

### 13 ***Plasma and Brain Metabolite Analysis***

14 Male Wistar rats (200 to 250g bodyweight) were anaesthetised using  
15 isoflurane in oxygen. Twenty MBq of  $^{18}\text{F}$ -GE-180 was administered intravenously by  
16 bolus injection into a tail vein of each rat. The rats were allowed to recover from the  
17 anesthesia. At the point of sacrifice, the rats were further anaesthetised and then  
18 sacrificed by cervical dislocation at 10, 30 or 60min post-injection (n=3 per time-  
19 point). Blood and brain were immediately collected for processing and HPLC  
20 analysis (full details of the methods in supplementary materials).

### 21 ***Immunohistochemistry***

22 For all the rats used for the PET study, astrogliosis and microglial activation  
23 were checked by immunohistochemistry staining for GFAP and CD11b respectively  
24 (detailed method in supplementary material).

## 1        ***Autoradiography***

2             $^{18}\text{F}$ -GE-180 (240.3GBq/ $\mu\text{mol}$ ; 1 nM) autoradiography was performed using  
3 20 $\mu\text{m}$  brain sections. Using adjacent sections, we assessed specific binding for  
4 TSPO by adding an excess of unlabelled R-PK11195 or unlabelled GE-180 (20 $\mu\text{M}$ ).  
5 Sections were pre-incubated in Tris buffer (Trizma preset crystals (Sigma, UK)  
6 adjusted at pH 7.4 at 4°C or room temperature, 50mM, with 120mM NaCl) at 4°C for  
7 5min, then incubated for 60min in Tris buffer at room temperature and then were  
8 rinsed twice for 5min with unlabelled buffer, followed by a quick wash in unlabelled  
9 distilled water and dried before exposition onto Phosphor-Imager screen for 2h.  
10 Autoradiographs were visualized using AIDA software (Raytest GmbH, Germany).

## 11        ***Statistical Analysis***

12            Paired Wilcoxon test were used to compare  $^{11}\text{C}$ -R-PK11195 vs  $^{18}\text{F}$ -GE-180  
13 uptake values for each ROI and to compare between ROIs for each tracer using 40  
14 to 60min post-injection sum-images. Unpaired Mann-Whitney test was used to  
15 compare the  $^{18}\text{F}$ -GE-180 uptake values with and without injection of unlabelled  
16 tracers from 40 to 60min post-injection sum-images. All statistics were performed  
17 with Statview 5.0.1 software, SAS Institute Inc., Cary, NC, USA. All data are  
18 expressed as mean $\pm$ SD.

## 19        **RESULTS**

### 20        ***Infarct Volumes***

21            As assessed by MRI, all animals but one had infarcts involving the whole  
22 striatum, and to some extent part of the cortical areas, most often the piriform cortex  
23 (Figure 1). One animal was excluded of the study based on the very small infarct  
24 observed on the T2 images (red dot, Figure 1A). The average infarct volumes

1 without this animal were  $65.7 \pm 12.7 \text{mm}^3$  and  $66.8 \pm 63.0 \text{mm}^3$  for the striatum and the  
2 cortical infarct respectively and  $132.5 \pm 61.9 \text{mm}^3$  total infarct.

### 3 ***PET Imaging***

4 As shown Figure 2, the uptake of  $^{18}\text{F}$ -GE-180 was significantly higher (+24%)  
5 in the core of the infarct than  $^{11}\text{C}$ -R-PK11195, and significantly lower (-18%) in the  
6 contralateral ROI than  $^{11}\text{C}$ -R-PK11195 uptake, leading to a significant improvement  
7 of  $1.5 \pm 0.2$  fold of the core to contralateral ratio (Figure 2D).  $^{18}\text{F}$ -GE-180 brain uptake  
8 in normal animals ( $0.082 \pm 0.026\%$ ) was not significantly different than in the  
9 contralateral ROI ( $0.104 \pm 0.016\%$ ) of stroke animals. Using ROIs drawn on the T2  
10 MRI images to quantify the PET images yield the same results (See supplementary  
11 Figures 1) although automatic PET segmentation was able to detect intermediate  
12 level of TSPO expression on the edges of the infarct core (supplementary Figures 2),  
13 ROIs that could not be identified on anatomical MRI.

14 Using the Simplified Reference Tissue Model, we found that the binding  
15 potential ( $\text{BP}_{\text{ND}}$ ) of  $^{18}\text{F}$ -GE-180 was significantly higher than  $^{11}\text{C}$ -R-PK11195  $\text{BP}_{\text{ND}}$  in  
16 the core of the ischemic lesion ( $5.3 \pm 1.2$  vs.  $2.8 \pm 0.7$ ). However,  $R_1$  ( $= \frac{k_1}{k'_1}$ ; tracer  
17 delivery ratio between the chosen ROI and the reference ROI) values were above 1  
18 for both tracers in the lesion core suggesting faster delivery than in the reference  
19 (healthy) tissue. To account for this, we measured the  $\text{BP}_{\text{ND}}$  with a  $R_1$  value fixed to  
20 1. This significantly reduced the  $\text{BP}_{\text{ND}}$  for both tracers but the difference between the  
21  $\text{BP}_{\text{ND}}$  for  $^{18}\text{F}$ -GE-180 and  $^{11}\text{C}$ -R-PK11195 remained significant ( $3.5 \pm 0.4$  vs.  $2.4 \pm 0.5$ ).

22 Injection of an excess of unlabelled ligand significantly displaced  $^{18}\text{F}$ -GE-180  
23 in the infarct ( $69\% \pm 5\%$  and  $63\% \pm 4\%$  of the uptake before injection of the unlabelled  
24 ligand for R-PK11195 or GE-180, respectively) (Figure 3 and Table 1). Injection of

1 unlabelled ligands reduced significantly mean uptake values between 40-60min in  
2 the striatal infarct and those were not statistically different from contralateral ROIs  
3 (Table 1). Uptake values in the contralateral side post-injection of unlabelled R-  
4 PK11195 or GE-180 were not affected by injection of unlabelled tracer (Table 1),  
5 confirming that the contralateral tissue was void of specific binding, and could  
6 therefore be used as reference tissue for modelling.

### 7 ***Plasma and Brain Metabolite Analysis***

8 Following intravenous administration of  $^{18}\text{F}$ -GE-180, the percentage of  
9 radioactivity in the plasma that was due to the presence of parent compound  
10 decreased with time, such that 21% remained by 60min post-injection (Table 2).  
11 Radiolabelled metabolite M1, accounted for 21% of the total activity in the plasma  
12 10min post-injection, with the proportion increasing with time to 53% by 60min post-  
13 injection. Two other more minor metabolites were observed 10 or 30min after the  
14 intravenous administration of  $^{18}\text{F}$ -GE-180 increasing to 5 or 21% of total plasma  
15 activity by 60min post-injection. In contrast, the metabolites observed in the plasma  
16 are neither formed in the CNS nor cross the blood brain barrier to any significant  
17 degree. In the brain not less than 95% of the radioactivity was attributable to the  
18 parent compound, even 60min after administration (Table 2).

### 19 ***Immunohistochemistry and Autoradiography***

20 The immunohistochemistry revealed the presence of CD11b positive cells  
21 (activated microglial cells and infiltrated macrophages) in the core of the lesion and  
22 GFAP positive cells (astrogliosis) on the edge of the core ischaemic lesion (Figure  
23 4). TSPO binding was confirmed in vitro by autoradiography using  $^{18}\text{F}$ -GE-180 (1nM)  
24 and specificity of the binding was confirmed by displacement with excess of  
25 unlabelled R-PK11195 or GE-180 (1 $\mu\text{M}$ ) (Supplementary Figure 3).

## 1 **DISCUSSION**

2           As we have recently demonstrated in animal models [24], or even more so in  
3 human conditions where high inter-individual variability in term of size and/or  
4 localisation of the infarct is expected [36;37], direct comparison of the PET tracers in  
5 the same subject by performing successive scans within 24h is the most robust way  
6 of comparing the performance of two tracers such as  $^{18}\text{F}$ -GE-180 and  $^{11}\text{C}$ -R-  
7 PK11195.

8           In our study,  $^{18}\text{F}$ -GE-180 has a significantly higher uptake in the infarct and  
9 importantly a lower uptake in the healthy tissue, leading to a significantly better  
10 infarct/contralateral ratio, than  $^{11}\text{C}$ -R-PK11195. Interestingly, the fact that uptake  
11 values in the contralateral ROI ( $0.108\pm 0.018\%$ ) were not significantly different from  
12 control animals ( $0.082\pm 0.026\%$ ) and that injection of an excess of unlabelled R-  
13 PK11195 or GE-180 yielded identical values to those obtained without displacement  
14 (Table 1) demonstrates that the contralateral ROI did not contain specific binding  
15 and could therefore be used as reference tissue. In the ischemic striatum, the  
16 average uptake values (sum image 40-60min) were not significantly different from  
17 the contralateral ROI (Table 1) following injection of an excess of unlabelled R-  
18 PK11195 or GE-180, but the time-activity curve showed that the uptake values were  
19 not identical to those observed in the contralateral ROI either. This suggests that  
20 there is higher level of non-specific binding in the infarct and/or that a small fraction  
21 of the metabolites may have entered the brain through the disrupted brain blood  
22 barrier (BBB). Our metabolites study shows that  $^{18}\text{F}$ -GE-180 has blood  
23 pharmacokinetics similar to other new TSPO tracers such as  $^{11}\text{C}$ -DPA-713 or  $^{18}\text{F}$ -  
24 DPA-714, with 70%, 40% and 21% of the parent compound still present at 10min,  
25 30min and 60min post-injection respectively [38;39]. Similar to many of the new

1 TSPO tracers, metabolites were barely detectable in the healthy brain, supporting  
2 the fact that quantification of TSPO using  $^{18}\text{F}$ -GE-180 reflects the level of TSPO  
3 expression unbiased by non-specific uptake of metabolites. We cannot however  
4 exclude the possibility that some metabolites crossed the *disrupted* BBB post-stroke.  
5 This is supported by the modelling the data using the SRTM which showed  $R_1 > 1$ ,  
6 supporting faster tracer delivery in the infarct likely due to post-stroke brain blood  
7 barrier disruption that we have previously demonstrated [24].

8         Regarding the potential effect of a repeated administration of a non-tracer  
9 dose (1mg/kg) of TSPO ligands, we did not observe systematic change for each  
10 animals in TSPO binding 6 days post-MCAO (2<sup>nd</sup> scans) following administration of  
11 cold ligand at 5 days post-MCAO, which suggests that this dose of cold ligand did  
12 not affect the expression of TSPO. Assessing the potential effect of repeated  
13 administration of unlabelled ligand at doses used for displacement studies (1-  
14 5mg/kg), similar to those used for therapeutic use for example, was outside the  
15 scope of the present work and would require further characterisation.

16         Our modelling data confirmed the raw uptake data and showed  $1.5 \pm 0.2$  fold  
17 higher BP values for  $^{18}\text{F}$ -GE-180 than for  $^{11}\text{C}$ -R-PK11195. The localisation and  
18 specificity of the binding was also confirmed by in vitro autoradiography, and  
19 coincided with an increased number of activated microglial cells and infiltrated  
20 macrophages in the infarct, and an astrocytic scar around it as shown by the  
21 immunohistochemistry.

22         Overall, the results presented here are in good agreement with those recently  
23 published by Dickens et al. [1] using a different model of neuroinflammation and  
24 support further use of  $^{18}\text{F}$ -GE-180 in preclinical and clinical imaging of TSPO.  
25 Although  $^{11}\text{C}$ -R-PK11195 is still widely used clinically and preclinically [16;22;40], the

1 present results are in line with previous observation made by our group and others  
2 with different tracers supporting the use of  $^{18}\text{F}$ -labelled tracers providing better  
3 signal-to-noise ratio and also longer half-life allowing off-site use. It should be noted  
4 however that both Dickens *et al.* [1] study and ours use models of strong and acute  
5 neuroinflammation, it would therefore be desirable to assess the second generation  
6 of TSPO tracers, such as [ $^{18}\text{F}$ ]GE-180, [ $^{18}\text{F}$ ]DPA-714, [ $^{18}\text{F}$ ]PBR111 or  
7 [ $^{18}\text{F}$ ]FEDAA1106 and many others [16;22] which have demonstrated improved  
8 signal-to-noise ratio when compared to [ $^{11}\text{C}$ ]PK11195, using other types of model  
9 (e.g. multiple sclerosis, transgenic model of Alzheimer's disease) inducing lower  
10 level of inflammation that are more challenging to detect.

## 11 **CONCLUSION**

12 The use of successive scans with  $^{11}\text{C}$ -R-PK11195 and  $^{18}\text{F}$ -GE-180 has  
13 allowed us to truly compare the 2 tracers in the same animals, hence avoiding  
14 potential bias due to inter-individual variability frequently observed in model such as  
15 the stroke model in rats. We were able to demonstrate here that  $^{18}\text{F}$ -GE-180 is a  
16 strong candidate for TSPO imaging with an improved signal-to-noise ratio and lower  
17 non-specific signal when compared to  $^{11}\text{C}$ -R-PK11195.

18



## 1 **DISCLOSURE**

2           This study was supported by GE healthcare Limited. GE healthcare Ltd was  
3 involved in the design of the study and performed the metabolites analysis. GE  
4 healthcare Ltd was not involved in other experiments.

## 5 **ACKNOWLEDGMENTS**

6           This work was supported by GE Healthcare Ltd, the Wolfson Molecular  
7 Imaging Centre, Manchester and the European Union's Seventh Framework  
8 Programme (FP7/2007-2013) under grant agreement n°HEALTH-F2-2011-278850  
9 (INMiND). The authors wish to thanks the personnel of the Wolfson Molecular  
10 Imaging Centre, especially Miss Gemma Chapman and Messrs Marc Radigois and  
11 Michael Green for facilitating this study. The Bioimaging Facility microscopes used in  
12 this study were purchased with grants from BBSRC, Wellcome Trust and the  
13 University of Manchester Strategic Fund; thanks go to Peter March, Jane Kott and  
14 Robert Fernandez for running the Bioimaging Facility.

## 1 REFERENCES

- 2 (1) Dickens AM, Vainio S, Marjamaki P, Johansson J, Lehtiniemi P, Rokka J, et al.  
3 Detection of Microglial Activation in an Acute Model of Neuroinflammation Using  
4 PET and Radiotracers 11C-(R)-PK11195 and 18F-GE-180. *J Nucl Med.* 2014;55:466-72.
- 5 (2) Denes A, Thornton P, Rothwell NJ, Allan SM. Inflammation and brain injury: acute  
6 cerebral ischaemia, peripheral and central inflammation. *Brain Behav Immun.*  
7 2010;24:708-23.
- 8 (3) McColl BW, Allan SM, Rothwell NJ. Systemic inflammation and stroke: aetiology,  
9 pathology and targets for therapy. *Biochem Soc Trans.* 2007;35:1163-5.
- 10 (4) Heneka MT, O'Banion MK, Terwel D, Kummer MP. Neuroinflammatory processes in  
11 Alzheimer's disease. *J Neural Transm.* 2010;117:919-47.
- 12 (5) Johnston H, Boutin H, Allan SM. Assessing the contribution of inflammation in  
13 models of Alzheimer's disease. *Biochem Soc Trans.* 2011;39:886-90.
- 14 (6) Lee YJ, Han SB, Nam SY, Oh KW, Hong JT. Inflammation and Alzheimer's disease. *Arch*  
15 *Pharm Res.* 2010;33:1539-56.
- 16 (7) Holmes C, Cunningham C, Zotova E, Woolford J, Dean C, Kerr S, et al. Systemic  
17 inflammation and disease progression in Alzheimer disease. *Neurology.* 2009;73:768-  
18 74.
- 19 (8) Akiyama H, Barger S, Barnum S, Bradt B, Bauer J, Cole GM, et al. Inflammation and  
20 Alzheimer's disease. *Neurobiol Aging.* 2000;21:383-421.
- 21 (9) Lee JK, Tran T, Tansey MG. Neuroinflammation in Parkinson's disease. *J*  
22 *Neuroimmune Pharmacol.* 2009;
- 23 (10) Gerhard A, Pavese N, Hotton G, Turkheimer F, Es M, Hammers A, et al. In vivo  
24 imaging of microglial activation with [11C](R)-PK11195 PET in idiopathic Parkinson's  
25 disease. *Neurobiol Dis.* 2006;21:404-12.
- 26 (11) Long-Smith CM, Sullivan AM, Nolan YM. The influence of microglia on the  
27 pathogenesis of Parkinson's disease. *Prog Neurobiol.* 2009;89:277-87.
- 28 (12) Tansey MG, McCoy MK, Frank-Cannon TC. Neuroinflammatory mechanisms in  
29 Parkinson's disease: potential environmental triggers, pathways, and targets for  
30 early therapeutic intervention. *Exp Neurol.* 2007;208:1-25.
- 31 (13) Ringheim GE, Conant K. Neurodegenerative disease and the neuroimmune axis  
32 (Alzheimer's and Parkinson's disease, and viral infections). *J Neuroimmunol.*  
33 2004;147(1-2):43-9.
- 34 (14) Banati RB, Newcombe J, Gunn RN, Cagnin A, Turkheimer F, Heppner F, et al. The  
35 peripheral benzodiazepine binding site in the brain in multiple sclerosis: Quantitative

- 1 in vivo imaging of microglia as a measure of disease activity. *Brain*.  
2 2000;123(11):2321-37.
- 3 (15) Oh U, Fujita M, Ikonomidou VN, Evangelou IE, Matsuura E, Harberts E, et al.  
4 Translocator protein PET imaging for glial activation in multiple sclerosis. *J*  
5 *Neuroimmune Pharmacol*. 2011;6:354-61.
- 6 (16) Chauveau F, Boutin H, Van CN, Dolle F, Tavitian B. Nuclear imaging of  
7 neuroinflammation: a comprehensive review of [11C]PK11195 challengers. *Eur J Nucl*  
8 *Med Mol Imaging*. 2008;35:2304-19.
- 9 (17) Venneti S, Lopresti BJ, Wiley CA. The peripheral benzodiazepine receptor  
10 (Translocator protein 18kDa) in microglia: From pathology to imaging. *Prog*  
11 *Neurobiol*. 2006;80:308-22.
- 12 (18) Pappata S, Cornu P, Samson Y, Prenant C, Benavides J, Scatton B, et al. PET study of  
13 carbon-11-PK 11195 binding to peripheral type benzodiazepine sites in glioblastoma:  
14 a case report. *J Nucl Med*. 1991;32:1608-10.
- 15 (19) Turkheimer FE, Edison P, Pavese N, Roncaroli F, Anderson AN, Hammers A, et al.  
16 Reference and target region modeling of [11C]-(R)-PK11195 brain studies. *J Nucl*  
17 *Med*. 2007;48:158-67.
- 18 (20) Foldersma H, Boellaard R, Vandertop WP, Kloet RW, Lubberink M, Lammertsma AA,  
19 et al. Reference tissue models and blood-brain barrier disruption: lessons from (R)-  
20 [11C]PK11195 in traumatic brain injury. *J Nucl Med*. 2009;50:1975-9.
- 21 (21) Kropholler MA, Boellaard R, van Berckel BN, Schuitemaker A, Kloet RW, Lubberink  
22 MJ, et al. Evaluation of reference regions for (R)-[(11)C]PK11195 studies in  
23 Alzheimer's disease and mild cognitive impairment. *J Cereb Blood Flow Metab*.  
24 2007;27:1965-74.
- 25 (22) Dolle F, Luus C, Reynolds A, Kassiou M. Radiolabelled molecules for imaging the  
26 translocator protein (18 kDa) using positron emission tomography. *Curr Med Chem*.  
27 2009;16:2899-923.
- 28 (23) Tang D, McKinley ET, Hight MR, Uddin MI, Harp JM, Fu A, et al. Synthesis and  
29 structure-activity relationships of 5,6,7-substituted pyrazolopyrimidines: discovery of  
30 a novel TSPO PET ligand for cancer imaging. *J Med Chem*. 2013;56:3429-33.
- 31 (24) Boutin H, Prenant C, Maroy R, Galea J, Greenhalgh AD, Smigova A, et al. [<sup>18</sup>F]DPA-  
32 714: direct comparison with [<sup>11</sup>C]PK11195 in a model of cerebral ischemia in rats.  
33 *PLoS ONE*. 2013;8:e56441.
- 34 (25) Doorduyn J, Klein HC, Dierckx RA, James M, Kassiou M, de Vries EF. [(11)C]-DPA-713  
35 and [(18)F]-DPA-714 as New PET Tracers for TSPO: a comparison with [(11)C]-(R)-  
36 PK11195 in a rat model of herpes encephalitis. *Mol Imaging Biol*. 2009;11:386-98.

- 1 (26) Takano A, Piehl F, Hillert J, Varrone A, Nag S, Gulyas B, et al. In vivo TSPO imaging in  
2 patients with multiple sclerosis: a brain PET study with [18F]FEDAA1106. *EJNMMI*  
3 *Res.* 2013;3:30-3.
- 4 (27) Takano A, Arakawa R, Ito H, Tateno A, Takahashi H, Matsumoto R, et al. Peripheral  
5 benzodiazepine receptors in patients with chronic schizophrenia: a PET study with  
6 [11C]DAA1106. *Int J Neuropsychopharmacol.* 2010;13:943-50.
- 7 (28) Wadsworth H, Jones PA, Chau WF, Durrant C, Fouladi N, Passmore J, et al. [(1)F]GE-  
8 180: a novel fluorine-18 labelled PET tracer for imaging Translocator protein 18 kDa  
9 (TSPO). *Bioorg Med Chem Lett.* 2012;22:1308-13.
- 10 (29) Calamante F, Lythgoe MF, Pell GS, Thomas DL, King MD, Busza AL, et al. Early  
11 changes in water diffusion, perfusion, T1, and T2 during focal cerebral ischemia in  
12 the rat studied at 8.5 T. *Magn Reson Med.* 1999;41:479-85.
- 13 (30) Wegener S, Weber R, Ramos-Cabrer P, Uhlenkueken U, Sprenger C, Wiedermann D,  
14 et al. Temporal profile of T2-weighted MRI distinguishes between pannecrosis and  
15 selective neuronal death after transient focal cerebral ischemia in the rat. *J Cereb*  
16 *Blood Flow Metab.* 2006;26:38-47.
- 17 (31) Camsonne R, Crouzel C, Comar D, Maziere M, Prenant C, Sastre C, et al. Synthesis of  
18 N-(11-C) Methyl, N-(Methyl-1 Propyl), (Chloro-2 Phenyl)-1 Isoquinoleine  
19 Carboxamide-3 (PK 11195): a new ligand for peripheral benzodiazepine receptors. *J*  
20 *Labelled Comp Radiopharm.* 1984;21:985-91.
- 21 (32) Cremer JE, Hume SP, Cullen BM, Myers R, Manjil LG, Turton DR, et al. The  
22 distribution of radioactivity in brains of rats given [N-methyl-11C]PK 11195 in vivo  
23 after induction of a cortical ischaemic lesion. *Int J Rad Appl Instrum B.* 1992;19:159-  
24 66.
- 25 (33) Maroy R, Boisgard R, Comtat C, Frouin V, Cathier P, Duchesnay E, et al. Segmentation  
26 of rodent whole-body dynamic PET images: an unsupervised method based on voxel  
27 dynamics. *IEEE Trans Med Imaging.* 2008;27:342-54.
- 28 (34) Maroy R, Boisgard R, Comtat C, Jago B, Fontyn Y, Jan S, et al. Quantitative organ time  
29 activity curve extraction from rodent PET images without anatomical prior. *Med*  
30 *Phys.* 2010;37:1507-17.
- 31 (35) Cawthorne C, Prenant C, Smigova A, Julyan P, Maroy R, Herholz K, et al.  
32 Biodistribution, pharmacokinetics and metabolism of interleukin-1 receptor  
33 antagonist (IL-1RA) using [(18) F]-IL1RA and PET imaging in rats. *Br J Pharmacol.*  
34 2011;162:659-72.
- 35 (36) Gerhard A, Schwarz J, Myers R, Wise R, Banati RB. Evolution of microglial activation  
36 in patients after ischemic stroke: a [11C](R)-PK11195 PET study. *Neuroimage.*  
37 2005;24:591-5.

- 1 (37) Thiel A, Radlinska BA, Paquette C, Sidel M, Soucy JP, Schirrmacher R, et al. The  
2 temporal dynamics of poststroke neuroinflammation: a longitudinal diffusion tensor  
3 imaging-guided PET study with 11C-PK11195 in acute subcortical stroke. *J Nucl Med.*  
4 2010;51:1404-12.
- 5 (38) Boutin H, Chauveau F, Thominiaux C, Gregoire MC, James ML, Trebossen R, et al.  
6 11C-DPA-713: a novel peripheral benzodiazepine receptor PET ligand for in vivo  
7 imaging of neuroinflammation. *J Nucl Med.* 2007;48:573-81.
- 8 (39) Chauveau F, Van Camp N, Dolle F, Kuhnast B, Hinnen F, Damont A, et al. Comparative  
9 evaluation of the translocator protein radioligands 11C-DPA-713, 18F-DPA-714, and  
10 11C-PK11195 in a rat model of acute neuroinflammation. *J Nucl Med.* 2009;50:468-  
11 76.
- 12 (40) Hughes JL, Jones PS, Beech JS, Wang D, Menon DK, Aigbirhio FI, et al. A microPET  
13 study of the regional distribution of [11C]-PK11195 binding following temporary  
14 focal cerebral ischemia in the rat. Correlation with post mortem mapping of  
15 microglia activation. *Neuroimage.* 2012;59:2007-16.  
16  
17

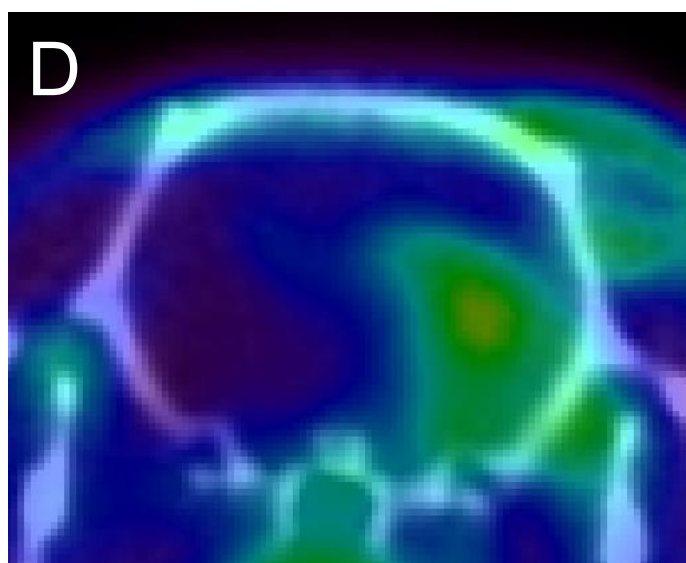
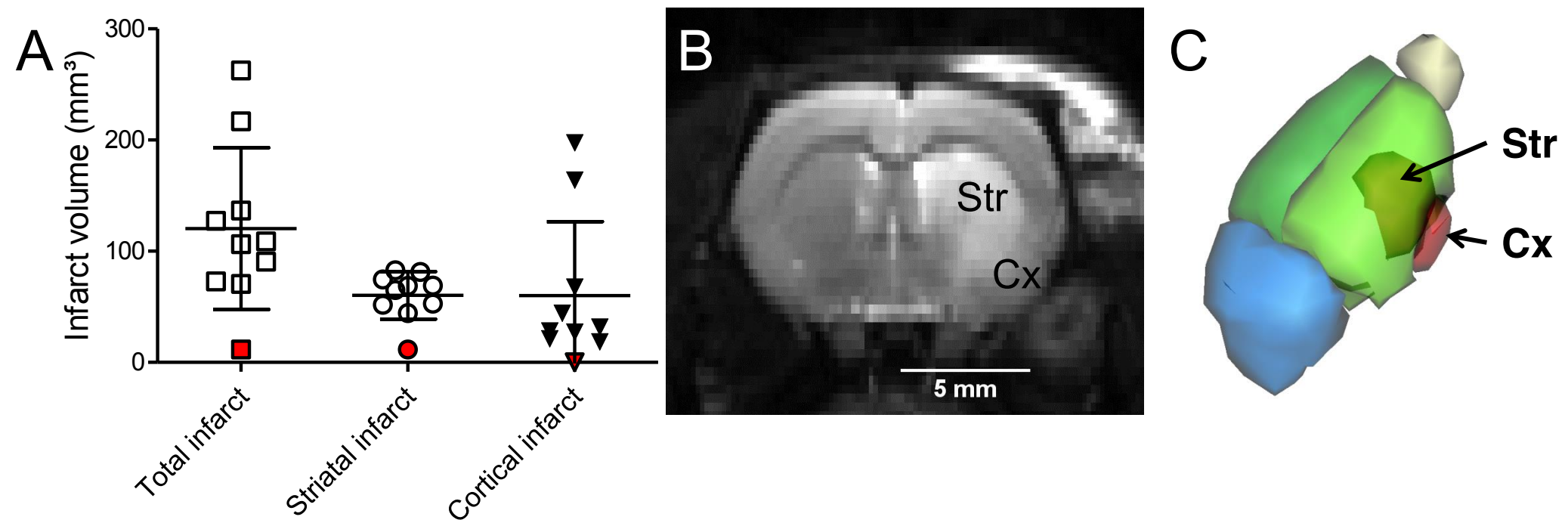
1 **Figure 1: (A)** Infarct volume (in mm<sup>3</sup>, mean±SD, n=10) as measured by T2 MRI  
2 imaging 24h post-MCAO, the red point represent the only animal excluded of the  
3 PET study based on the lack of infarct; **(B)** representative T2 MR image of a rat with  
4 the infarct visible as an oedematous area with enhanced contrast (white); **(C)** 3D  
5 rendering of the infarct areas measured on the animal shown in **(B)** with the cortical  
6 (Cx) and striatal (St) infarct shown in red and by transparency through the ipsilateral  
7 healthy tissue (light green), the contralateral (Contra) side is shown in dark green,  
8 the cerebellum and olfactory bulbs are shown in light yellow. Co-registered  
9 quantitative PET-CT images of the same animal (sum PET image between 40-60min  
10 post-injection) for <sup>11</sup>C-PK11195 **(D)** and <sup>18</sup>F-GE180 **(F)**.

11 **Figure 2:** <sup>11</sup>C-R-PK11195 uptake **(A)** and <sup>18</sup>F-GE-180 **(B)** (in %ID/cm<sup>3</sup>, mean±SD)  
12 over 60min post-injection in the infarct core and the contralateral side showing a  
13 higher difference between the lesion core and contralateral ROI for <sup>18</sup>F-GE-180 when  
14 compared to <sup>11</sup>C-R-PK11195 (6.1 fold vs 4.0 fold respectively). **(C)** Quantification of  
15 the tracer uptakes on sum-image between 40-60min post-injection showing a  
16 significantly lower uptake in the healthy tissue (dark green plot) and a significantly  
17 higher uptake in the lesion for <sup>18</sup>F-GE-180 (dark red plot), leading to a significant  
18 difference in core/contralateral ratio **(D)**. \* indicates significant differences between  
19 groups (n=6), paired Wilcoxon test, p<0.05.

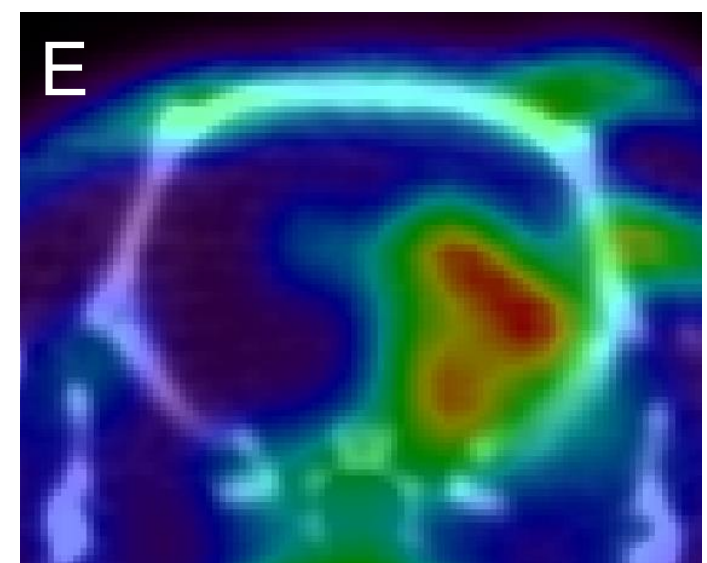
20 **Figure 3:** Time-activity curves of <sup>18</sup>F-GE-180 in the ipsilateral (infarcted) striatum  
21 and contralateral side before (0-20min) and after (>20min) intravenous injection of an  
22 excess of unlabelled PK11195 **(A)** or GE-180 **(B)** (1mg/kg) (n=3, same animals  
23 scanned at 5 and 6 days post-MCAO). ROIs were drawn on the T2 MR images 24h  
24 post-MCAO.

1 **Figure 4:** Representative immunohistochemical staining of microglial and infiltrated  
2 macrophages with CD11b (red), astrocytes with GFAP (green) and nuclear staining  
3 with DAPI in the contralateral (left panel) and ipsilateral (right panel) sides of the  
4 brain of a rat 6 days post-MCAO. From top to bottom, scale bars represent 200µm,  
5 100µm and 50µm. The insert (top-right panel) shows the approximate localisation of  
6 the field of view used for the immunohistochemistry (white rectangles) on the MRI  
7 and [<sup>18</sup>F]GE-180 autoradiographic image from the same animal.

Figure 1



$^{11}\text{C-R-PK11195}$



$^{18}\text{F-GE-180}$





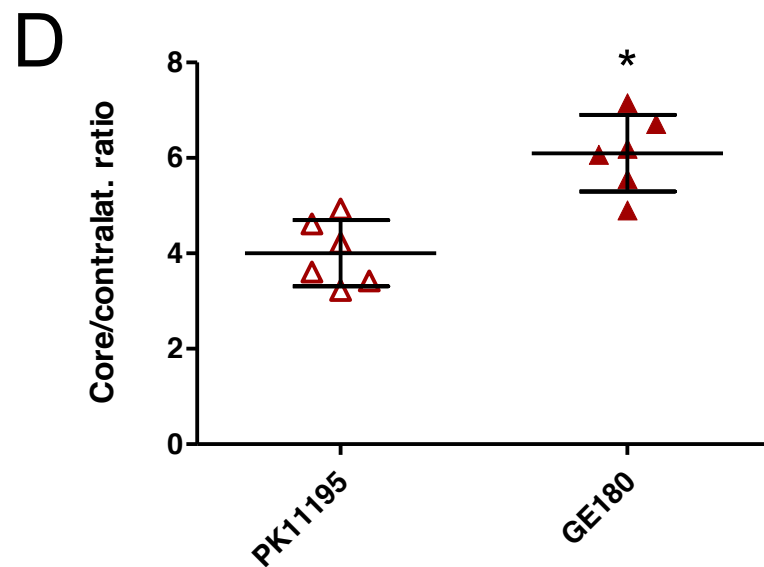
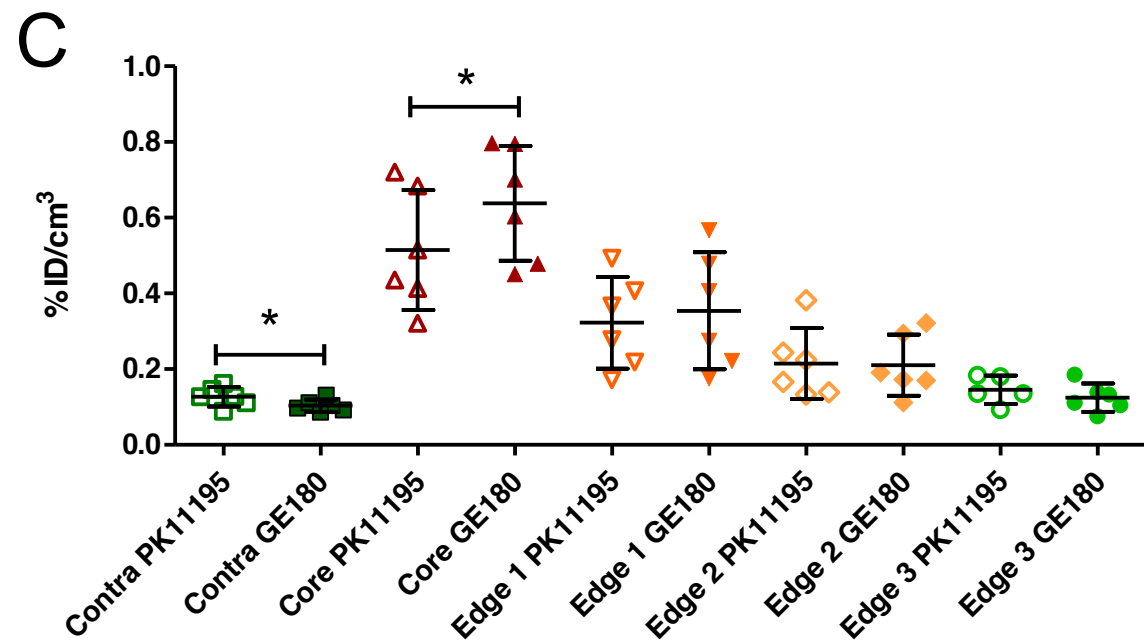
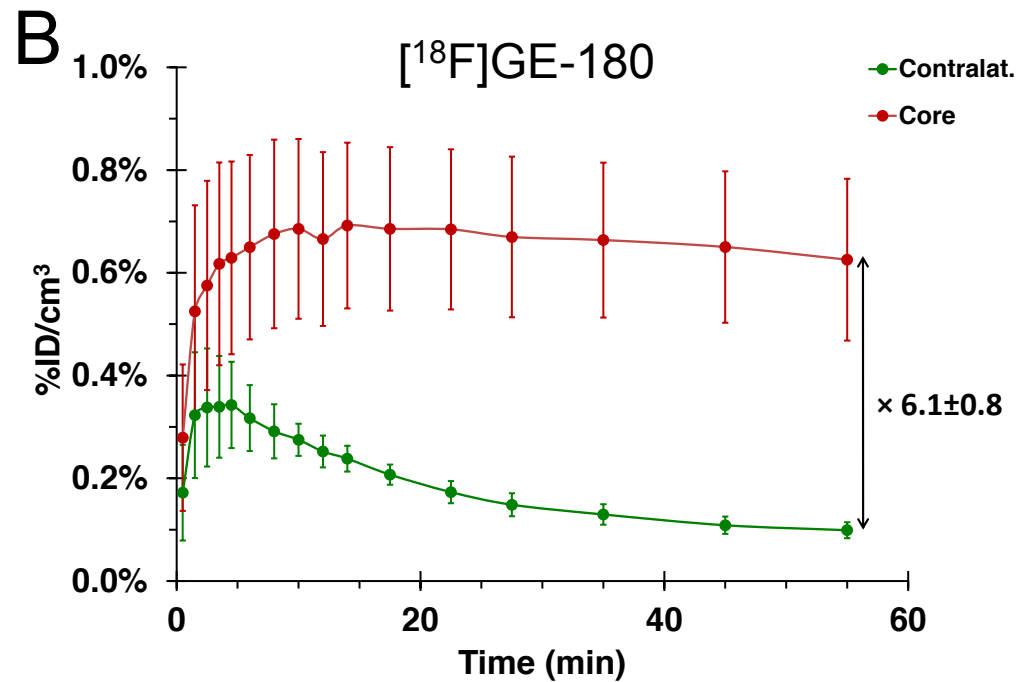
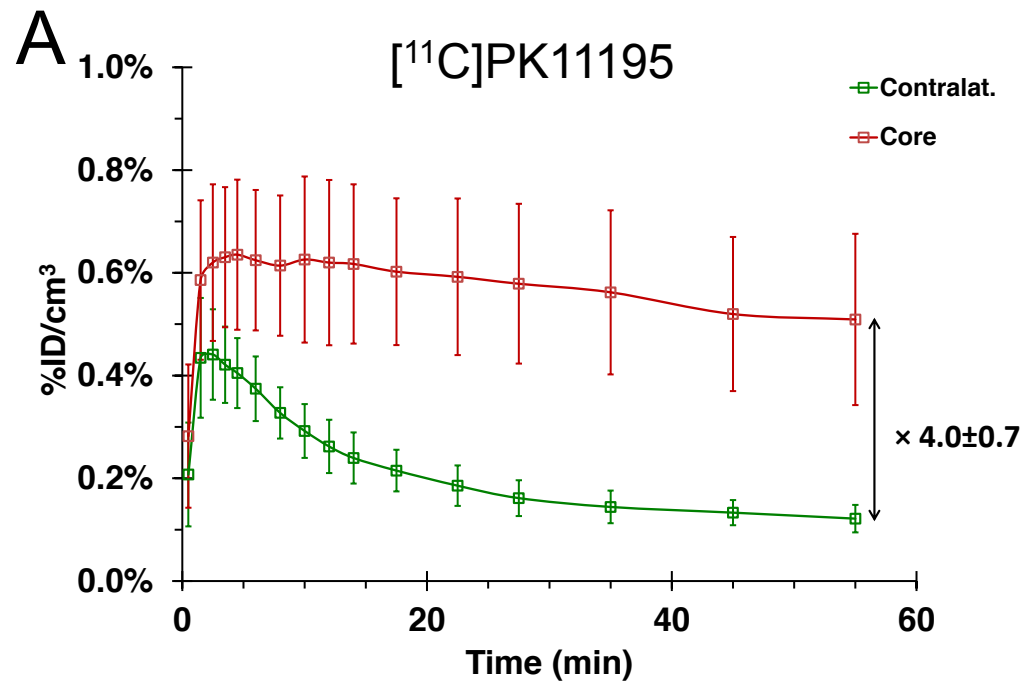


Figure 2

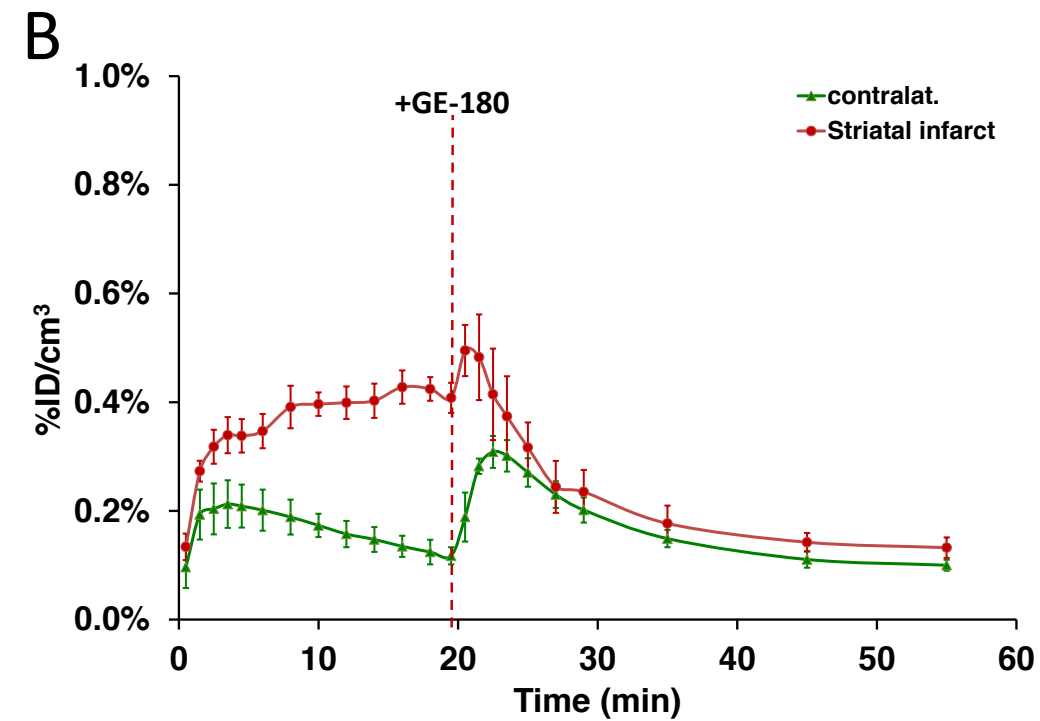
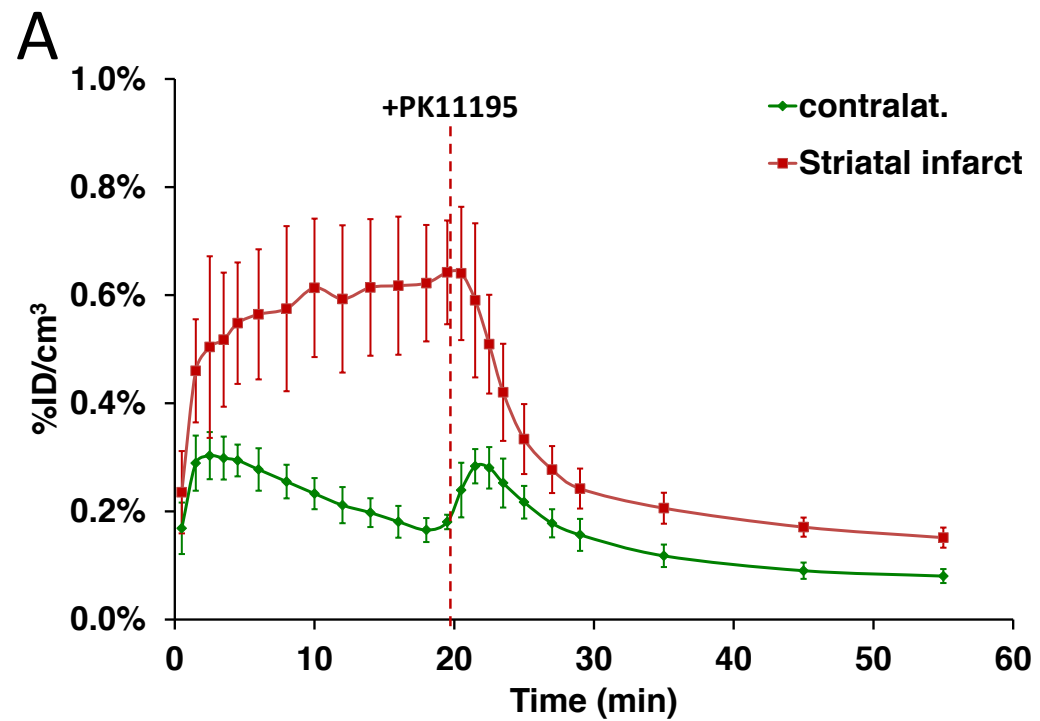


Figure 3

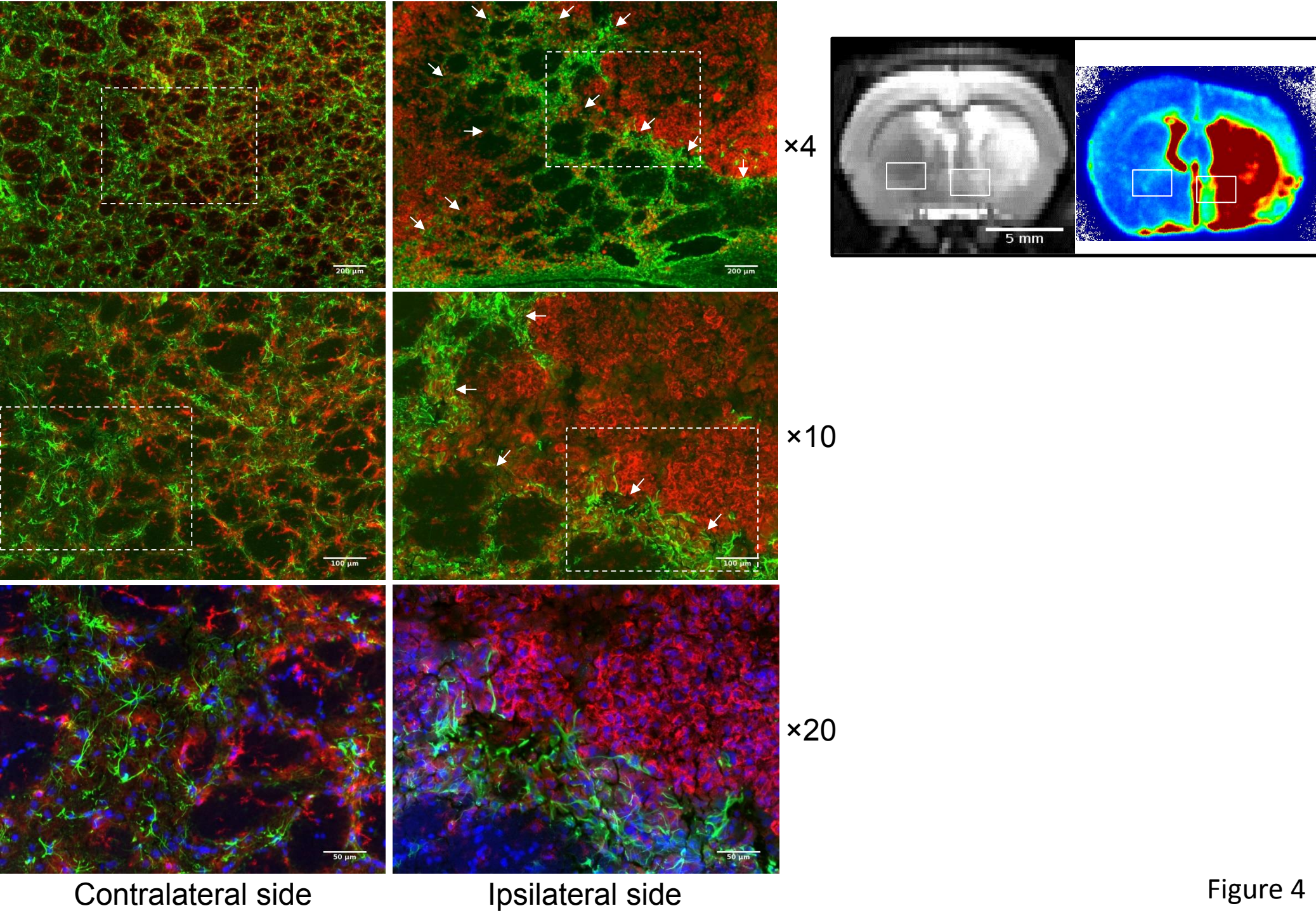
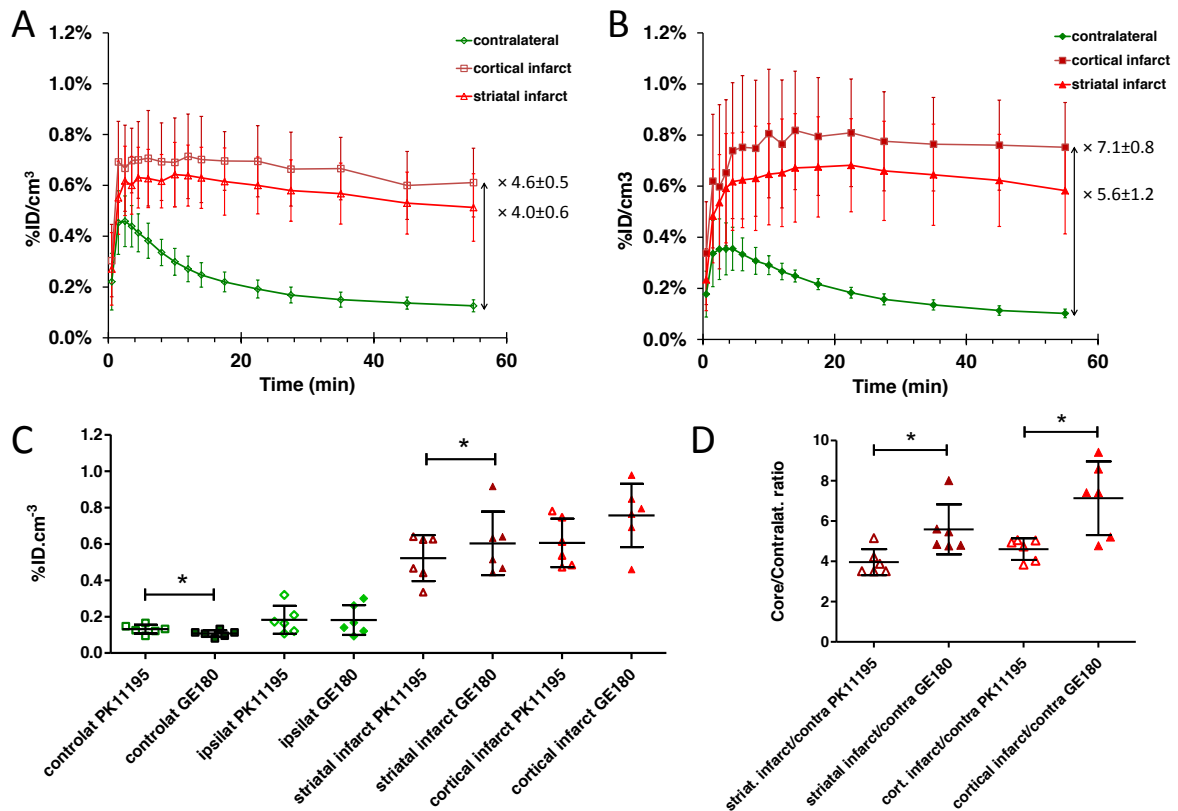


Figure 4

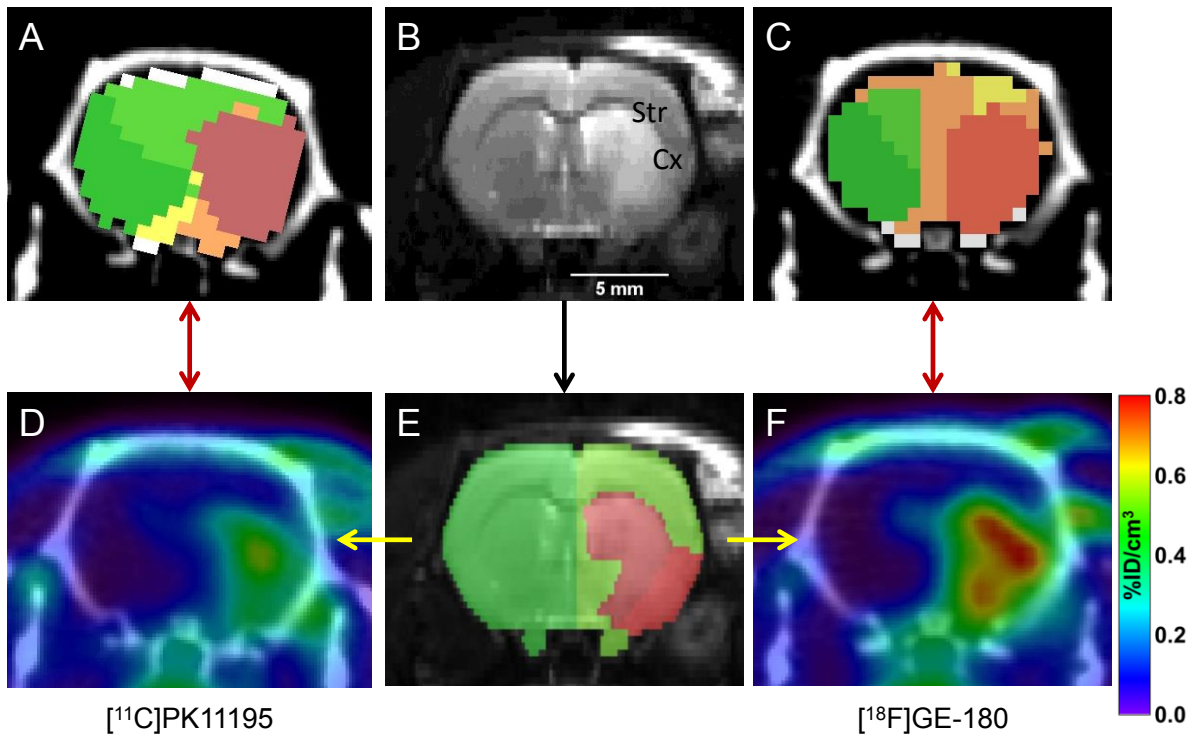
## SUPPLEMENTARY DATA

**Supplementary Table 1:** Injected dose and specific activity and amount of tracer injected for  $^{11}\text{C}$ -R-PK11195 and  $^{18}\text{F}$ -GE-180. Data are expressed as mean $\pm$ SD (min-max).

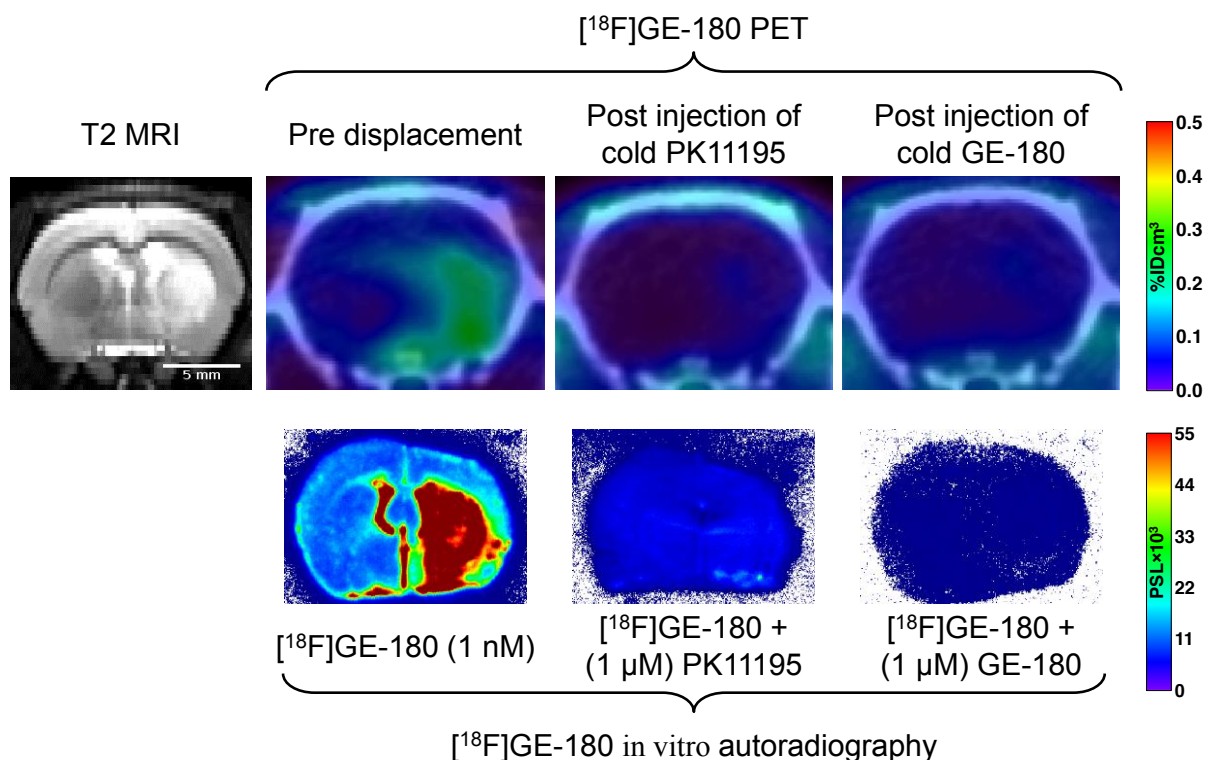
<b>Baseline study</b>	<b><math>^{11}\text{C}</math>-R-PK11195</b>	<b><math>^{18}\text{F}</math>-GE-180</b>
Injected doses (MBq)	27.93 $\pm$ 10.88 (15.42-47.84)	27.87 $\pm$ 8.70 (18.89-40.34)
Amount of tracer injected (nmol)	0.83 $\pm$ 0.66 (0.22-2.10)	0.34 $\pm$ 0.35 (0.09-0.94)
Specific activity (GBq/ $\mu\text{mol}$ )	52.44 $\pm$ 37.68 (11.21-111.00)	178.41 $\pm$ 130.77 (20.01-364.76)
<b>Displacement study</b>	<b><math>^{18}\text{F}</math>-GE-180+R-PK11195</b>	<b><math>^{18}\text{F}</math>-GE-180+GE-180</b>
Injected doses (MBq)	31.59 $\pm$ 1.39 (29.99-32.49)	31.79 $\pm$ 2.78 (28.90-34.46)
Amount of tracer injected (nmol)	0.54 $\pm$ 0.32 (0.35-0.91)	0.68 $\pm$ 0.75 (0.12-1.53)
Specific activity (GBq/ $\mu\text{mol}$ )	69.98 $\pm$ 30.31 (35.46-92.24)	123.85 $\pm$ 109.26 (20.94-238.52)



**Supplementary Figure 1:** <sup>11</sup>C-R-PK11195 uptake (**A**) and <sup>18</sup>F-GE-180 (**B**) (in %ID/cm<sup>3</sup>, mean±SD, n=6 per group) over 60min post-injection in the cortical and striatal infarct as delineated on the T2 MRI and the contralateral side showing a higher difference between the infarct ROIs and contralateral ROI for <sup>18</sup>F-GE-180 when compared to <sup>11</sup>C-R-PK11195 (5.6 to 7.1 fold vs 4.0 to 4.6 fold respectively). This can be attributed to a significantly lower uptake in the healthy tissue and a significantly higher uptake in the lesion for <sup>18</sup>F-GE-180 as shown by comparison of the <sup>18</sup>F-GE-180 and <sup>11</sup>C-R-PK11195 uptake (**C**; from sum-image between 40 and 60min post-injection), leading to a significant difference in infarct/contralateral ratio (**D**). \* Indicates significant differences between groups, Wilcoxon test, p<0.05.



**Supplementary Figure 2:** PET images were quantified using two sets of ROI: **(A)** & **(C)** show the ROIs obtained with the automatic segmentation of the dynamic PET images, displayed next to the T2-weighted MR image **(B)** showing good correlation between the localisation of the PET segmented ROIs and the lesion seen on the MRI. Quantitative PET-CT images (sum PET image between 40-60min post-injection) for  $^{11}\text{C}$ -R-PK11195 **(D)** and  $^{18}\text{F}$ -GE180 **(F)**. **(E)** shows infarct ROIs as delineated on the T2-weighted MRI and also used to quantify the PET images. Both sets of ROIs gave similar results (see Figure 2 and Supplementary Figure 1).



**Supplementary Figure 3:** Representative images of the displacement of <sup>18</sup>F-GE-180 by an excess of unlabeled PK11195 or GE-180 in vivo by PET (top panel) and ex vivo by autoradiography (bottom panel) from the same animal. For the PET study, <sup>18</sup>F-GE-180 was displaced by an excess of unlabeled PK11195 or GE-180 (1mg/kg) injected 20min post-injection of <sup>18</sup>F-GE-180. In vitro, brain sections were incubated with <sup>18</sup>F-GE-180 (1nM) alone or in presence of 1μM of unlabeled PK11195 or GE-180. Top panel, from left to right: co-registered coronal view of the T2 MRI and PET-CT images pre-displacement (17-20min post-injection of <sup>18</sup>F-GE-180 sum-image) and post-displacement (40-60min sum-image). Bottom panel: autoradiographic images of adjacent brain sections from the same animal (PSL= photostimulated luminescence per pixel).

## **Methods**

### **Induction of Focal Cerebral Ischaemia in Rats**

Focal cerebral ischaemia was induced by 60min transient occlusion of the right middle cerebral artery (MCAO) by the insertion of a monofilament (DOCCOL Corp.) under isoflurane anaesthesia (induction 4% and maintained 1.5% in 70% N<sub>2</sub>O and 30% O<sub>2</sub> mixture) as described by Longa et al. (1). Core body temperature was maintained throughout the procedure at 37.0±0.5°C by a heating blanket (Homeothermic Blanket Control Unit; Harvard Apparatus Limited). After 60min, the filament was withdrawn to restore CBF. Success and reproducibility of the MCAO was verified by assessment of the infarct size by MRI as described below.

### **Magnetic Resonance Imaging**

Parameters for the FLASH-TOF-2D sequence were: TR=15.0ms, TE=3.8ms, single echo, matrix=256x256, number of averages=2, FOV=4cm with 120 slices of 0.4mm with an inter-slice distance of 0.25mm, giving a final voxel size of 0.156×0.156×0.25mm. Parameters for the T<sub>2</sub>-weighted fast spin echo sequence based on RARE (2) were: repetition time=4.8s, base echo time=20ms, effective echo time=60 ms, number of echos=8, number of samples=256, number of views=128, number of averages=2 with 25 slices of 1mm, giving a final voxel size of 0.156×0.312×1mm.

### **Positron Emission Tomography**

#### *Data acquisition*

The scans were performed on a Siemens Inveon® PET-CT scanner. The acquisition protocol consisted of the following parameters: a CT scan was performed



prior the PET acquisition to obtain the attenuation correction factors, the time coincidence window was set to 3.432ns and the levels of energy discrimination were set to 350keV and 650keV. The list mode acquisition data files were histogrammed into 3D sinograms with a maximum ring difference of 79 and span 3. The list mode data of the emission scans were sorted into 16 dynamic frames (5×1min, 5×2min, 3×5min, 3×10min). Finally, the emission sinograms (each frame) were normalized, corrected for attenuation, scattering and radioactivity decay, and reconstructed using OSEM3D (16 subsets and 4 iterations) into images of dimensions 128<sup>2</sup> (transaxially) × 159 (longitudinally) with 0.776×0.776×0.796mm voxels (FOV diameter: 99.3mm × 126.6mm longitudinally).

### **Plasma and Brain metabolite Analysis**

Blood was collected and transferred to an Eppendorf tube and then centrifuged at 3500×g to obtain plasma. The brain was removed from the skull and immediately placed on ice. All samples were immediately transferred on wet ice for processing and HPLC analysis.

Plasma was added to ice cold acetonitrile (1:10 v/v) and centrifuged at 16000×g for 3min to remove the proteins, to allow the measurements of the total amount of free radioactivity (using the organic precipitation by centrifugation technique).

The brain (without the cerebellum and medulla/pons) was homogenized with 10ml of ice-cold acetonitrile using a rotary blade homogeniser at maximum speed for approximately 1min. The homogenate was centrifuged at 4500×g for 5min to remove the proteins to allow the measurements of the total amount of free radioactivity (using the organic precipitation by centrifugation technique).

Following centrifugation, the supernatant was transferred to a round bottom flask and removed by rotary evaporation at 40°C, followed by reconstitution with 2.5ml of mobile phase. This solution was then filtered through a 0.22µm filter. One ml of this reconstituted sample was then injected onto the HPLC system for analysis. The HPLC system comprised a Gilson 322 binary pump with a Gilson UV/Vis-156 detector, BGO coincident detector, Bioscan flow counter and a Rheodyne 7125 manual injector. The rotary evaporator used was a VWR RV 10 digital rotary evaporator and water bath with a Buchi vacuum controller V-850 pump. Centrifuges used were the Eppendorf centrifuge 5804 R and the Eppendorf centrifuge 5415 D (for processing the plasma and brain samples respectively). Tissue homogenisation was performed using a CAT x120 homogeniser. Radioactivity was counted using the Wallac 1480 Wizard gamma counter.

A 1 ml aliquot of sample (after protein precipitation) was manually injected into the injector and analysed using a mBondapak C18 semi prep column on a isocratic method running over a 20min run time. The mobile phase consisted of 60% acetonitrile and 40 % water at a flow rate of 3ml/min. Radioactivity detection was via a dual BGO coincident radioactive detector with a 500µl loop and a bioscan flow count. The ultraviolet (UV) absorbance was captured with an UV/Vis detector set at a wavelength of 230nm. A universal chromatography interface (UCI) was used to convert the electronic signal to digital data. All HPLC chromatograms were captured and peaks were manually identified and then integrated using the Dionex HPLC software (Chromeleon version 6.6). The area under the curve (AUC) was integrated for each peak from the radioactive trace and then expressed as the percentage of the total peak area. At the beginning and end of each study day, an aliquot of mobile phase (60% acetonitrile and 40% of water) spiked with [<sup>18</sup>F]GE-180 and was

analysed on the HPLC system. This was used as a reference point for the retention time of the parent peak in the in vivo samples. In addition, non-radioactive reference standard was added as a spike into each biological sample and used as an internal standard to further confirm the relative retention time ( $t_r$ ) of the parent peak. The data were collected from 3 studies ( $n=3$ ) where one animal per sample point was used, except for the 60min post-injection plasma and brain samples, where tissue or blood from 2 animals was combined.

### **Immunohistochemistry**

For all the procedure described below Phosphate Buffered saline (PBS) at 100mM was used. Frozen rat brain sections were post-fixed in paraformaldehyde (4% in PBS) for 30min and washed (6×5min) in PBS. Sections were permeabilized with 30min of incubation in 0.1% Triton X-100 containing 2% normal donkey serum in PBS to block non-specific binding. Without further washing, sections were incubated overnight at 4°C with primary antibodies in 2% normal donkey serum/0.1% Triton X-100 in PBS. Double immunohistochemistry staining was performed against glial fibrillary acidic protein (GFAP) with rabbit anti-cow GFAP (Dako, 1:1000) and CD11b (Ox42) with mouse anti-rat CD11b (Serotec, 1:1000). Sections were then washed (3×10min) in PBS and incubated for 2h at room temperature with secondary antibodies (AlexaFluor 488nm donkey anti-mouse IgG, AlexaFluor 594nm donkey anti-rabbit IgG (Molecular Probes, Invitrogen)), all 1:500 in 2% normal donkey serum/0.1% Triton X-100 in PBS) and then washed again (3×10min) in PBS. Sections were mounted with a Prolong Antifade kit (Molecular Probes, Invitrogen); those incubated without the primary antibodies served as negative controls.

Images were collected on a Olympus BX51 upright microscope using a 4×/0.13, 10×/0.30 or 40×/0.50 UPlanFLN objectives and captured using a Coolsnap

ES camera (Photometrics) through MetaVue Software (Molecular Devices). Specific band pass filter sets were used to prevent bleed through from one channel to the next. Images were then processed and analysed using ImageJ (<http://rsb.info.nih.gov/ij>).

## References

- (1) Longa EZ, Weinstein PR, Carlson S, Cummins R. Reversible middle cerebral artery occlusion without craniectomy in rats. *Stroke*. 1989;20:84-91.
- (2) Hennig J, Nauerth A, Friedburg H. RARE imaging: a fast imaging method for clinical MR. *Magn Reson Med*. 1986;3:823-833.